Biomineralization in the Palaeozoic oceans: Evidence for simultaneous crystallization of high and low magnesium calcite by phacopine trilobites

Martin R. Lee[a]✉, Clare Torney[a]*, Alan W. Owen[a]
[a]*School of Geographical and Earth Sciences, University of Glasgow, Gregory Building, Lilybank Gardens, Glasgow G12 8QQ, Scotland, UK.*
*Current address: *Historic Scotland Conservation Directorate, 7 South Gyle Crescent, Edinburgh, EH12 9EB*

✉Corresponding author at: *School of Geographical and Earth Sciences, University of Glasgow, Gregory Building, Lilybank Gardens, Glasgow G12 8QQ, Scotland, UK. Tel:* Tel: +44(0)141-330-2634, fax: +44(0)141-330-4817. E-mail: Martin.Lee@glasgow.ac.uk

ABSTRACT
The chemical composition and microstructure of the calcite cuticles of eleven species of phacopine trilobites has been investigated by electron beam imaging, diffraction, and microanalysis, and results reveal that the lenses of their schizochroal eyes differed significantly in chemical composition from the rest of the cuticle *in vivo*. Apart from the eye lenses, most cuticles are inferred to have escaped extensive recrystallization because their constituent crystals are sub-micrometre in size and have a preferred orientation that is consistent between species. Their current compositions of ~1.4 to 2.4 mole% $MgCO_3$ are likely to be close to original values, although as they commonly luminesce and contain detectable manganese and iron, some diagenetic alteration has taken place. The associated lenses have a microstructure that is suitable for focusing light, yet are optically turbid owing to the presence within calcite of micropores and crystals of microdolomite, apatite, celestite and pyrite. The microdolomite indicates that lenses recrystallized from an original high-Mg calcite composition and this is supported by the presence of nanometre-scale modulated microstructures in both the calcite and dolomite. These lenses currently contain ~1 to 6 mole% $MgCO_3$, and by comparison with the proportion of magnesium lost from echinoderm stereom in the same thin sections, may have contained ~7.5 mole% $MgCO_3$ *in vivo*. In some samples, more extensive diagenetic alteration is evidenced by recrystallization of the cuticle including lenses to coarse equant calcite or enrichment of the cuticle, but not necessarily the lenses, in magnesium accompanying replacement by a Mg-Fe phyllosilicate. The phacopine trilobites had to modify partition coefficients for magnesium considerably in order to grow lenses with contrasting compositions to the rest of their cuticles, and such a strong vital effect on biomineralization suggests that incorporation of magnesium was essential for functioning of their calcite optical systems.

Keywords: Trilobite, microdolomite, eye, high-Mg calcite, cuticle

1. Introduction

Many Palaeozoic invertebrates used low-Mg calcite (Mg/Ca <0.04), high-Mg calcite (Mg/Ca >0.04) or aragonite to construct their shells and cuticles (e.g. Zhuravlev and Wood, 2008; Porter, 2010). Most previous workers have concluded that trilobite cuticles were made solely from low-Mg calcite given the good preservation of their finely crystalline microstructures (James and Klappa, 1983) and results of chemical and isotopic analyses that are inconsistent with the former presence of diagenetically unstable aragonite or high-Mg calcite (James and Klappa, 1983; Wilmot and Fallick, 1989; Brand, 2004). Despite this apparent consensus, there have been a number of suggestions that cuticles contained higher concentrations of magnesium. Teigler and Towe (1975) arrived at this conclusion by analogy with the ostracodes, and Lowestam (1963) recorded up to 5 mole% $MgCO_3$ from a Carboniferous (Lower Pennsylvanian) cuticle. McAllister and Brand (1989a) suggested that cuticles of analysed Ordovician and Devonian species originally contained 'intermediate' magnesium calcite with ~2 to 7 mole% $MgCO_3$ because when plotted in Sr/Ca–Mg space their compositions fall between those of 'articulate' brachiopods (originally low-Mg calcite) and crinoids (originally high-Mg calcite). This suggestion was supported by the finding of Lee et al. (2007) that the lenses of schizochroal trilobite eyes may also have contained elevated concentrations of magnesium *in vivo*. It is crucial therefore to assess the degree of diagenetic alteration of lenses in trilobite eyes and their adjacent cuticles to determine their *in vivo* chemical compositions if the associated biology is to be understood.

The eyes are one of the few parts of the trilobite cuticle for which their specialised function and importance is unequivocal. The structure of the schizochroal eyes of the Ordovician-Devonian trilobite suborder Phacopina is unique in the animal Kingdom (e.g. see Clarkson et al., 2006 for a review) and there is considerable controversy about how these eyes operated. Much of the debate centers on how confidently original microstructures and compositions can be distinguished from those that may be diagenetic in origin (e.g. Miller and Clarkson, 1980; Bruton and Haas, 2003; Clarkson et al., 2006; Schoenemann and Clarkson, 2011). One focus of these discussions has been on the existence or otherwise of a doublet structure within each lens; the shape of the boundary between the two components leading to comparisons being made by Clarkson and Levi-Setti (1975) with optical systems designed by Des Cartes and Huygens in the 17th Century. Lee et al. (2007) found that lenses in the sample of *Dalmanites* sp. previously investigated by Clarkson and Levi-Setti (1975) were composed of low-Mg calcite with micrometre-sized inclusions of dolomite. They used this as evidence that parts of the lenses originally crystallized as high-Mg calcite and speculated that these internal compositional differences enhanced the optical properties. Although this finding potentially has very important implications for understanding the detailed functioning of schizochroal eyes, the precise stratigraphical age and provenance of the analysed specimen is unknown and the question remains as to how widespread within the phacopine trilobites high-Mg calcite lenses were. It is also possible that the dolomite in the *Dalmanites* sp. sample could have formed during diagenetic alteration of its host rock and so is unrelated to original lens compositions. Here we report results of a compositional study of eleven phacopine species of different ages and from various localities. A finding that dolomite is a common constituent of lenses, but is absent from the rest of the cuticle and host rock, will demonstrate that phacopine trilobites simultaneously crystallized calcite of substantially different compositions. Such a conclusion would have important implications for understanding biological controls on

mineralization within the Palaeozoic oceans, and the function of the eyes themselves.

2. Materials and methods

2.1. Trilobites

The eleven species of phacopine trilobites used in this study are listed in Table 1 along with their stratigraphic positions and source localities. The sample set includes multiple specimens of a single species collected from the same locality, which enables an assessment of the degree of variability in diagenetic alteration of cuticles within a rock unit. For these specimens the thin section number is given in parentheses after the species name. In addition, different species from the same locality were studied in order to evaluate the extent of taxonomic control on the composition and microstructure of the cuticle.

The cuticles of phacopine trilobites include a pair of compound or aggregate 'schizochroal' eyes, each of which typically consists of a few tens of lenses with a maximum diameter of about 1 mm (Clarkson et al., 2006) (Fig. 1a). The lenses are separated by cuticular material (sclera) and are covered by a thin outer cornea (Fig. 1b). When viewed in cross-section they may appear as doublets with a curved interface between the upper unit and the intralensar bowl; the upper unit may also contain a variably diffuse central core (Fig. 1b) (see Clarkson et al., 2006 and references therein). Petrographic thin sections were cut normal to the visual surface of the eye and in a 'horizontal' plane approximately parallel to the palpebral lobe so that each will contain lenses together with associated sclera, part of the adjacent cuticle and some host rock (Fig. 1a). Ideally the plane of each thin section will therefore be coincident with the lens axis, so that most of the lens calcite will be oriented with its *c* axis in the plane of the thin section and with one of its *a* axes normal to the plane of the thin section (Fig. 1c).

2.2. Imaging

The thin sections were characterised initially by light microscopy, then studied by cathodoluminescence (CL) using a Cambridge Image Technology (CITL) instrument operated at 20 kV/500 nA. After the thin sections had been coated with carbon, backscattered electron (BSE) images were acquired using a FEI Quanta 200F field emission environmental scanning electron microscope (FEG-ESEM) operated in high-vacuum (10^{-5} Pa) mode, at 20 kV and with a high beam current. After removal of the conductive carbon coating, secondary electron (SE) images were additionally obtained from some of the thin sections using the FEG-ESEM operated in low vacuum (~60 Pa). Under these instrumental conditions image contrast arises from spatial variations in charge accumulation across the sample surface, and these 'charge contrast' (CC) images can reveal intracrystalline variations in trace element concentration at much higher spatial resolutions than achievable by optical or SEM cathodoluminescence (e.g. Lee et al., 2008). In order to measure the sizes of dolomite crystals within lens calcite, thin sections of eight of the species were etched in 1% HCl for 20 seconds then gold coated for SE imaging at high vacuum.

2.3. X-ray microanalysis

Quantitative chemical analyses were obtained from carbon coated thin sections analysed using two instruments. One dataset was acquired with a Cameca SX100 electron probe (EP) operated at 15 kV/40

nA and with a 2-5 µm spot. Calibration used the following mineral standards: spinel (Mg), silicarb (Ca), Mn metal (Mn), fayalite (Fe), and celestite (Sr). Peak/background count times were 30/15 seconds and typical detection limits for the trace elements were 0.03 wt% $MnCO_3$, 0.02 wt% $FeCO_3$, and 0.09 wt% $SrCO_3$. As a large number of such analyses were needed to obtain representative compositions of the lenses, a subsequent dataset was acquired using a Zeiss Sigma field-emission analytical electron microscope (AEM) operated at 15 kV/9 nA. This instrument is equipped with two X-ray detectors, an Oxford Instruments X-Max 80 mm^2 silicon-drift energy dispersive (ED) detector and an INCA Wave wavelength-dispersive (WD) detector, both operated through an Oxford Instruments INCA microanalysis system. Calibration used mineral standards: periclase (Mg), calcite (Ca), rhodonite (Mn), hematite (Fe), and celestite (Sr). Calcium and magnesium were analysed using the ED detector with a 60 second count time, whereas manganese, iron and strontium were analysed using the WD detector employing LiF (Mn & Fe) and TAP (Sr) crystals. Peak/background count times were 30/15 seconds, giving typical detection limits for the trace elements of 0.06 wt % $MnCO_3$, 0.07 wt % $FeCO_3$ and 0.08 wt% $SrCO_3$. Beam currents were continuously monitored using a Faraday cup and analytical totals of 100 ± 2 wt% carbonate were obtained. For most cuticle analyses the beam was rastered over a 10 × 7 µm area, whereas a 28 × 19 µm raster was used for the more coarsely crystalline lenses. A range of raster sizes was employed for analyses of echinoderm stereom depending on the scale of the features of interest. All analytical results are expressed as mole% carbonate.

2.4. Electron backscatter diffraction

The microstructure of the cuticle and lenses was characterised by electron backscatter diffraction (EBSD) using an EDAX-TSL integrated ED-EBSD system running OIM version 5.2.1 software that is attached to the Quanta FEG-ESEM. Prior to EBSD work the thin sections were briefly polished with colloidal silica in order to enhance the quality of Kikuchi patterns, and they remained uncoated. EBSD maps were acquired in low vacuum (~60 Pa) mode with the microscope operated at 20 kV and using a relatively high beam current. Acquisition rates were betweeb 10 and 50 Kikuchi patterns/second. EBSD was used to determine the orientation of cuticle and lens calcite crystals over relatively large areas (i.e. tens of micrometres) and to help orient samples that were to be prepared for transmission electron microscopy (TEM) (see below). In samples containing both calcite and dolomite, EBSD mapping was also used to determine the orientation relationships of the two minerals. However, as the Kikuchi patterns of these minerals are too similar to be reliably distinguished by automated indexing on the EBSD software, a variant of the EBSD technique, Chemistry assisted Indexing (ChI), was used. ChI acquires compositional information by ED X-ray microanalysis simultaneously with the Kikuchi patterns so that orientation data can be filtered using calcium and magnesium concentrations for allocation to the correct minerals.

2.5. Transmission electron microscopy

The microstructures of calcite and dolomite within the lenses were characterised at higher resolutions using a FEI Tecnai T20 TEM operated at 200 kV. The electron-transparent (i.e. <~100 nm thick) foils required for the TEM work were prepared from lenses of three species by one of two methods. Foils were cut from thin sections of the lenses of *Geesops sparsinodosus* and *Dalmanites* sp. (TS1) using the

focused ion beam (FIB) technique (Lee et al., 2003) and employing a FEI Nova 200 Dualbeam FIB instrument operated with 30 kV Ga^+ ions. Each foil was cut to ~20 µm in length by 6 µm deep and 0.1 µm thick, then was lifted out from the surface of the thin section using an *in-situ* micromanipulator and welded to the tines of a copper holder with electron- and ion-deposited platinum. These foils were cut normal to the surface of the thin section and with the plane of the foil parallel to the lens axis, and so also parallel to the *c* axis of constituent calcite. For TEM work the foils were mounted in a double-tilt goniometer holder and were oriented such that the axes of rotation of the holder were normal and parallel to the calcite *c* axis. A larger foil was made from a *Reedops* cf. *cephalotes* lens in polished thin section by argon ion milling using a Gatan Duomill operated at 5 kV. In preparation for ion milling the thin section was mounted in Lakeside resin and a 3.05 mm diameter copper washer was secured to the surface of the thin section with its central 400 µm aperture positioned over the lens of interest. The washer with lens attached was then cut away and extracted from the rest of the thin section and ion milled until perforated. The plane of the foil is parallel to the calcite *c* axis so that during TEM work the electron beam will be oriented approximately normal to the *c* axis and so in the plane of the *a* axes. All foils were characterised by bright- and dark-field imaging and selected area electron diffraction (SAED), and the diffraction patterns were manually indexed using unit-cell parameters for calcite ($R\bar{3}c$: a= 0.4991 nm, b = 0.4991 nm, c = 1.7062 nm, β = 120º) and dolomite ($R\bar{3}$: a= 0.4807 nm, b = 0.4807 nm, c = 1.6010 nm, β = 120º). See Lee (2010) for a recent review of the TEM technique and its applications to the study of minerals and rocks.

3. Results

3.1. Non-lensar cuticle microstructure and chemical composition

EBSD mapping shows that the interlensar sclera of most specimens is composed of sub-micrometre to micrometer sized calcite crystals with a preferred orientation. Crystallographic orientations differ within the scleral pillar, and between the scleral pillar and the alveolar ring (Fig. 1b), but in regions of the cuticle beyond the eye, calcite *c* axes are oriented approximately normal to its inner and outer surfaces, as was observed by Teigler and Towe (1975). These parts of the cuticle in all three Moroccan specimens have been partially replaced by quartz (Klug et al., 2009) with the cuticles of *Austerops smoothops* and *Barrandeops granulops* additionally containing a Mg-Fe phyllosilicate (Fig. 2). Cuticles may be luminescent throughout, or adjacent to their inner and outer margins only, with non-luminescent calcite between. The non-lensar calcite cuticles of most species contain 0.7 to 2.4 mole% $MgCO_3$ with <0.1 mole% $MnCO_3$, variable but low $FeCO_3$ and up to 0.30 mole% $SrCO_3$ (Table 2, Fig. 3). Analyses of the two samples of *Geesops schlotheimi* show that the compositional variation within a single species at a single locality can be at least ~0.4 mole% $MgCO_3$ and ~0.4 mole% $FeCO_3$ (Table 2). All three samples from the Eifelian Trilobitenfelder locality (i.e. *Geesops sparsinodosus* and *Geesops schlotheimi* G33 and G42) have similar strontium concentrations (Fig. 3). The unusually low magnesium concentrations in the sample of *Boeckops boecki* cuticle may reflect its recrystallization during formation of enclosing calcite cements, which have a very similar magnesium-poor composition (see below). Those parts of the cuticle of the Moroccan samples *Austerops smoothops* and *Barrandeops granulops* that have escaped replacement by quartz or phyllosilicates have the highest concentrations of

both $MgCO_3$ and $SrCO_3$ (Fig. 3).

3.2. Lens microstructure, turbidity and CL properties

A detailed analysis of trilobite lens microstructures will be provided in a subsequent paper. Suffice it to note that the lenses studied here can be divided into three groups by microstructure. Lenses in the samples of *Dalmanites* sp. and *Odontochile hausmanni* contain elongate subgrains (trabeculae) whose boundaries fan out towards the lens base (Fig. 1b). Despite the presence of trabeculae the lens calcite displays unit extinction when viewed in transmitted light between crossed polarisers and EBSD confirms that its *c* axis is oriented parallel to the lens axis in all parts except within a few micrometres of the visual surface. Here the *c* axis of calcite fans outwards to lie a higher angle to the visual surface, producing a narrow 'radial fringe' (Fig. 1b). The majority of the other species studied have a much thicker radial fringe (Torney et al., 2008) and in the central and basal part of the lens the calcite *c* axis again lies parallel to the lens axis. In lenses of some of these species the *c* axis of calcite fans outwards towards the base of the lens. The third microstructure is seen only in the specimen of *Reedops cephalotes* whereby the lenses are composed of 10-40 μm sized equant calcite crystals with no preferred orientation (Fig. 4a).

The lenses of all samples studied apart from that of *Reedops cephalotes* contain optically turbid calcite, but the proportion of turbidity varies between species, between different samples of the same species, and between lenses of a single eye. In those lenses that are incompletely turbid the intralensar distribution of clear and turbid calcite commonly defines the 'core' and 'bowl' that are distinguished by either being significantly more or less turbid than the enclosing lens. Lenses of *Boeckops boecki*, *Odontochile hausmanni, Barrandeops granulops, Geesops sparsinodosus* and *Geesops schlotheimi* are uniformly turbid, whereas those of *Reedops* cf. *cephalotes* have an optically clear core (Fig. 4b) and *Austerops smoothops, Phacops* sp. and *Eldredgeops rana* lenses have bowls that are optically clear and free of mineral inclusions (Fig. 4c, d). Some *Dalmanites* sp. lenses are entirely turbid whereas in others the turbidity is restricted to the core and bowl (Lee et al., 2007). All lenses contain luminescent calcite, and some are uniformly luminescent whereas most other lenses contain patches of calcite that range from non-luminescent to bright orange. The distribution of calcite with different luminescence intensities shows little correspondence to the intralensar arrangement of clear and turbid calcite.

3.3. Lens mineralogy

Lee et al. (2007) found that the turbidity that defines the core and bowl of *Dalmanites* sp. is due to the presence within lens calcite of micropores and micrometer-sized dolomite crystals (hereafter 'microdolomite'). BSE imaging shows that micropores are ubiquitous in the turbid calcite of all lenses examined in the present study and they have microporosities, determined by point counting using the SEM, of 3 to 7 vol. %. Micropores are angular and their edges lie parallel to the $\{10\bar{1}4\}$ cleavage planes of calcite (Fig. 5a, 4b). Lenses of all species apart from *Reedops cephalotes* contain microdolomite together with much less abundant sub-micrometer sized crystals of apatite, celestite ($SrSO_4$) and framboidal pyrite (Fig. 5a, b). Microdolomite crystals are typically euhedral with a $\{10\bar{1}4\}$ habit and are either completely enclosed by calcite, or juxtaposed with micropores (Fig. 5b). In the *Dalmanites* sp. lenses, microdolomite crystals have well developed oscillatory zoning in CC images,

with zone boundaries oriented parallel to $\{10\bar{1}4\}$, and these images also reveal that the microdolomite crystals have grown into micropores (Fig. 5b). The average volume of microdolomite within the lenses of a sample, as determined by point counting of BSE images, ranges from 1 to 5 vol. %. but varies within lenses, between lenses of the same eye and between species (Table 3). Microdolomite crystal sizes were measured from SE images of acid-etched thin sections and within any one lens they range from sub-micrometer up to several tens of micrometers (Table 3), although part of this measured range will reflect a sectioning artifact (i.e. cutting the crystals through their edge *vs* center). The mean size of the microdolomite crystals differs between lenses of the same eye, and apart for *Dalmanites* sp. the range is typically 1.5 μm or less (Table 3). The inter-species variability of mean microdolomite sizes is less than the ~1.5 μm difference between lenses in one eye, although microdolomite crystals in the Moroccan trilobites are consistently small whereas the largest occur in *Boeckops boecki* (Fig. 5a) and *Dalmanites* sp. lenses (Table 3).

TEM imaging has provided further information on the microstructure of microdolomite and its crystallization (Figs 5c, d, 6a, b). The microdolomite has grown around preexisting apatite crystals (Fig. 5c) and into preexisting pore space (Fig. 6a). Where dolomite is completely enclosed by calcite it cross-cuts subgrain boundaries and contains small calcite inclusions (Fig. 6b). These relationships suggest that microdolomite crystallized after calcite, including its micropores, and apatite. SAED patterns from microdolomite and enclosing calcite show that the two minerals have the same crystallographic orientation (Fig. 6b), and EBSD mapping confirms that this common orientation holds true for the entire population of microdolomite and calcite crystals within any one lens. Microdolomite in the lenses of *Reedops* cf. *cephalotes, Geesops sparsinodosus* and *Dalmanites* sp. (TS1) was imaged by TEM and in all cases displays a nanometre-scale modulated microstructure that is comparable to that of calcian microdolomite from former high-Mg calcite echinoderm stereom (Blake et al., 1982; Reeder, 1992) (Fig. 5d, 6a, b). The zoning of *Dalmanites* sp. (TS1) microdolomite seen in CC is also apparent in TEM images of the same crystals, which demonstrates that the orientation and/or scale of the modulations is compositionally controlled (Fig. 5d). Lens calcite itself is composed of a mosaic of very slightly misoriented micrometer sized subgrains with planar and dislocation-rich boundaries (Fig. 7a). Patches within the calcite crystals contain modulations with a ~30 nm wavelength that produce the streaking between spots in corresponding SAED patterns (Fig. 7a, b). In one crystal the modulations are rotated by a twin plane, and as transmitted light imaging showed that its host lens contains $\{\bar{1}018\}$ *e* twins (Fig. 4b), it is likely that deformation twinning postdated formation of the modulations.

3.4. Lens chemical compositions

The mean chemical compositions of lenses are listed in Table 2, and these data have also been plotted in Figure 3. The samples analysed fall into three groups by their magnesium concentrations. Seven of the species have lenses that contain 1.5 to 2.4 mole% $MgCO_3$ whereas in the magnesium-rich group, which comprises the Moroccan species *Austerops smoothops*, *Barrandeops granulops* and *Phacops* sp., the lenses contain 5.4 to 6.2 mole% $MgCO_3$ (Table 2, Fig. 3). Equant calcite in the *Reedops cephalotes* lenses has the lowest magnesium concentrations of 1.2 mole% $MgCO_3$. Manganese concentrations are very low in all samples, whereas iron shows more variation, with *Geesops schlotheimi* lenses having relatively high concentrations (Table 2). Most of the magnesium-poor lenses have low strontium

concentrations and magnesium-rich lenses are correspondingly richer in strontium (Fig. 3), with the exception of *Geesops sparsinodosus* and *Geesops schlotheimi* lenses that are magnesium-poor and strontium-rich (Fig. 3). The compositions of *Austerops smoothops* and *Phacops* sp. lenses in Table 2 are from micropore- and inclusion-rich parts of the lenses whereas the optically clear bowls have compositions of $Ca_{96.35}Mg_{1.07}Mn_{0.07}Fe_{2.49}Sr_{0.02}CO_3$ (AEM; n = 2) and $Ca_{97.32}Mg_{0.48}Mn_{0.56}Fe_{1.58}Sr_{0.05}CO_3$ (AEM; n = 2) respectively and so differ considerably to their host lenses (Table 2). Only in *Boeckops boecki* lenses were the microdolomite crystals of sufficient size to yield an analysis uncontaminated by adjacent calcite (Fig. 5a), and results show that this microdolomite has a slightly calcian composition of $Ca_{107}Mg_{93}(CO_3)_2$.

3.5. Host rock mineralogy and composition

The trilobite samples studied are enclosed within a sandy limestone (mudstone or wackestone) matrix with the exception of *Boeckops boecki*, which is from a grainstone and whose cuticle is overgrown by radiaxial fibrous calcite cements that are in optical continuity with lens calcite. These cements are also turbid owing to the presence within calcite of 3.2 vol. % micropores and 0.4 vol. % microdolomite inclusions, and they have a composition of $Ca_{99.11}Mg_{0.86}Mn_{0.00}Fe_{0.01}Sr_{0.02}CO_3$ (EP; n= 15). ChI scan EBSD data demonstrate that within these cements the calcite and microdolomite share the same crystallographic orientation. Only in the *Eldredgeops rana* sample has the host rock been partially dolomitzed. These dolomite crystals are euhedral, ~10 to 103 μm in size, and only one crystal was found to have replaced the cuticle, and that was within sclera.

The host rocks of *Phacops* sp., two of the *Geesops schlotheimi* samples (G33RT and G42) and *Dalmanites* sp. (TS3) contain fragments of echinoderm stereom and these were investigated for any insights they might provide into the diagenetic alteration and original chemical composition of the associated trilobite cuticles. The stereom in the *Geesops schlotheimi* (G33RT and G42) and *Dalmanites* sp. (TS3) samples are composed of microporous calcite within inclusions of microdolomite and celestite, and are internally structureless (Fig. 8a). The fragment in the G33RT thin section (Fig. 8a) has a microporosity of 6.8 vol. %, contains 3.3 vol. % microdolomite, and EBSD shows that calcite and microdolomite crystals have a common crystallographic orientation. It has a composition of $Ca_{95.55}Mg_{3.39}Mn_{0.03}Fe_{0.89}Sr_{0.17}CO_3$ (AEM; n = 4), whereas the stereom fragment in the G42 thin section has a composition of $Ca_{97.16}Mg_{2.31}Mn_{0.02}Fe_{0.30}Sr_{0.21}CO_3$ (EP; n = 15). The stereom fragment in the *Dalmanites* sp. (TS3) thin section has a composition of $Ca_{96.28}Mg_{3.15}Mn_{0.18}Fe_{0.40}Sr_{0.00}CO_3$ (AEM; n = 6). In the *Phacops* sp. thin section the stereom fragment has retained more of its original internal structure (Fig. 8b, c). Where best preserved the stereom network is composed of calcite with very small micropores and microdolomite crystals, and analyses of 6 × 4 μm sized areas of the network yielded a composition of $Ca_{93.31}Mg_{6.15}Mn_{0.05}Fe_{0.35}Sr_{0.14}CO_3$ (AEM; n= 3). Analyses of larger (28 × 19 μm) areas that include the network and micropore- and inclusion-free calcite cement between (Fig. 8b) yielded compositions of $Ca_{94.44}Mg_{4.01}Mn_{0.21}Fe_{1.31}Sr_{0.03}CO_3$ (AEM; n= 4). In other parts of this stereom fragment the network is less well defined, its calcite contains coarser micropores and microdolomite crystals, and has a composition of $Ca_{93.95}Mg_{4.64}Mn_{0.19}Fe_{1.11}Sr_{0.11}CO_3$ (AEM; n= 2).

4. Discussion

4.1. Preservation of the non-lensar cuticle

Most non-lensar calcite cuticles are composed of micrometer sized crystals with a crystallographic preferred orientation that is consistent within and between species. The cuticles are therefore inferred to have escaped extensive recrystallization, which would be consistent with them having originally been low-Mg calcite, rather than aragonite or high-Mg calcite *in vivo*, in agreement with previous studies (James and Klappa, 1983; McAllister and Brand, 1989b; Wilmot and Fallick, 1989). One exception to this good microstructural preservation is seen in *Reedops cephalotes* where, together with lenses, it is composed of equant calcite crystals with no preferred orientation, indicating that the entire cuticle has been recrystallized. Wilmot (1990) noted that obliteration of primary microstructures accompanying recrystallization was "quite common" in trilobites from limestones and she attributed this relatively high reactivity to their originally finely crystalline microstructure. A similar diagenetic pattern was noted by McAllister and Brand (1989b), and Miller and Clarkson (1980) also described variable degrees of neomorphism of primary calcite in the cuticle and lenses of *Phacops* [now *Eldredgeops*] *rana milleri*.

Despite preservation of their fine-scale microstructures, the presence of manganese and iron in cuticles together with their luminescence suggests that they have been altered from their assumed manganese- and iron-free *in vivo* compositions. Wilmot (1990) also noted commonplace patchy alteration in a microstructural and CL study of trilobite cuticles, and found that luminescence may be limited to the inner and outer margins of the cuticle, indicating that transition metal ions were sourced from the host rock. Similar patterns of variations in CL emission intensity were found in the present study. Using wet chemical analyses of Middle Devonian *Phacops* [now *Eldredgeops*] *rana* cuticles, McAllister and Brand (1989a) showed a considerable range in the compositions of samples from a single rock unit indicating substantial variability in their degree of alteration. It is clear therefore that the trace element compositions of cuticles can be modified without dissolution-reprecipitation on a scale sufficient to change their original microstructures. It is not known whether these compositional modifications reflect fine-scale recrystallization of primary cuticle calcite, and/or cementation by authigenic calcite of primary intra- cuticle pores (e.g. canals; McAllister and Brand (1989b), Wilmot (1990)), or secondary intercrystalline porosity resulting from the decay of intraskeletal organic matter.

Given the evidence for diagenetic alteration from manganese and iron compositions, the concentrations of magnesium and strontium in non-lensar cuticle calcite may also have changed from original values. From an analytical study of *Phacops rana* cuticles within shale, McAllister and Brand (1989a) found that both magnesium and strontium both decrease with progressive diagenetic alteration of the cuticle. Their least altered samples contained ~2.7-2.9 mole% $MgCO_3$ and ~0.24-0.25 mole% $SrCO_3$. By applying that model to data collected in the present study, the three Eifelian Trilobitenfelder samples are inferred to have retained much of their original magnesium and strontium. The Morrocan samples *Austerops smoothops* and *Barrandeops granulops* have also retained their original strontium but their non-lensar cuticles are inferred to have gained magnesium during diagenesis because they lack microdolomite inclusions that would otherwise indicate that they recrystallized from an *in vivo* high-Mg calcite composition (see below). As the two Morrocan samples that have been enriched in magnesium also contain Mg-Fe phyllosilicates, the magnesium was probably introduced during this

partial replacement. The other samples analysed are interpreted to have lost both magnesium and strontium during diagenesis and so the inferred *in vivo* composition of the non-lensar calcite cuticles of phacopine trilobites is ~2.0 to 2.4 mole% $MgCO_3$ and ~0.2 to 0.3 mole% $SrCO_3$. These values are also consistent with Brand (2004), who described three Ordovician cuticles with a mean composition of $Ca_{97.63}Mg_{1.98}Mn_{0.09}Fe_{0.15}Sr_{0.15}CO_3$ and whose carbon, oxygen and strontium isotope values were comparable to those of coeval unaltered brachiopods.

4.2. Evidence for diagenetic alteration of lenses

All of the lenses studied are inferred to have been diagenetically altered to some extent, and with the exception of the sample of *Reedops cephalotes*, the main evidence for this diagenesis is turbidity of lens calcite caused by micropores and inclusions of microdolomite, apatite, celestite and pyrite. This turbidity cannot have been present *in vivo* because it would have significantly limited the transmission of light through the eye. As micropores, microdolomite, apatite and celestite are absent from the adjacent cuticle, the lenses are inferred to have followed a different diagenetic pathway, which can only have been due to substantial contrasts in their initial mineralogy and/or chemical composition. In common with the *Dalmanites* sp. sample described by Lee et al. (2007), lenses within the eyes of the other species included in the present study are inferred to have recrystallized because they originally contained high-Mg calcite. The primary evidence for a high-Mg calcite precursor is the presence of microdolomite, which has been described from former high-Mg calcite in ancient marine cements (Lohmann and Meyers, 1977), and in fossil echinoderm stereom (Leutoff and Meyers, 1984), stromatoporoids (Rush and Chafetz, 1991), rugose corals (Webb and Sorauf, 2002) and bryozoans (Taylor and Wilson, 1999). The full assemblage of low-Mg calcite plus micropores, microdolomite, celestite and pyrite found in most lenses is also very similar to the products of diagenetic alteration of Pennysylvanian high-Mg calcite ($Ca_{89}Mg_{11}CO_3$) echinoderm stereom described by Dickson (2001a). Micropores, microdolomite and celestite also occur within echinoderm fragments that were examined in the present study (Fig. 8a). The possibility that these microdolomite inclusions formed during more widespread dolomitization can be discounted because only the sample containing the *Eldredgeops rana* cuticle had been dolomitized, and this replacement was almost entirely restricted to the rock matrix.

The crystallographic orientation and microstructure of lens calcite and microdolomite lend further support to the suggestion that they had a high-Mg calcite precursor. As the present-day crystallographic orientation of the lens calcite is ideal for minimising birefringence and focusing light (Towe, 1973; Clarkson and Levi-Setti, 1975), it is reasonable to assume that *in vivo* lens orientations and microstructures have been largely retained. Such epitaxial replacement is the norm for recrystallization of high-Mg calcite to low-Mg calcite plus dolomite, which takes place by dissolution-reprecipitation across a narrow fluid film (e.g. Goldsmith, 1960; Blake et al., 1982; Grover and Kubanek, 1983; Dickson, 2001b). Microdolomite crystals share the crystallographic orientation of enclosing lens calcite on length scales ranging from adjacent crystals (as measured by SAED) to all of the microdolomite and calcite crystals within one lens (determined by EBSD). These same orientation relationships were found between the calcite and microdolomite formed by recrystallization of high-Mg calcite echinoderm stereom studied by Blake et al. (1982), Reeder (1992) and Dickson (2001a, b) as well as in the present study. The fine-scale modulated microstructure of lens microdolomite is also

comparable to that of the ~10 nm scale 'tweed' microstructure of calcian ($Ca_{108}Mg_{92}(CO_3)_2$) microdolomite crystals described by Blake et al. (1982), which had formed by recrystallization of Pennsylvanian echinoderm stereom (originally ~$Ca_{81}Mg_{19}CO_3$). As microdolomite crystals within lenses of the three species studied by TEM all have the same microstructure, a composition and origin comparable to that of microdolomite in the stereom is indicated. Lastly, the modulated microstructures of *Reedops* cf. *cephalotes* lens calcite are very similar to those described by Gunderson and Wenk (1981) for calcite ($Ca_{98.5}Mg_{0.9}Fe_{0.7}CO_3$) in Jurassic ooids. In this case the calcite contained two sets of modulations, one with a wavelength of 15 ± 5 nm and the other with an average wavelength of 50 nm, both of which were oriented parallel to $\{10\bar{1}4\}$, and generated streaks in corresponding SAED patterns, some of which were accompanied by additional reflections. Gunderson and Wenk (1981) concluded that the modulations formed from disordered calcite of a secondary origin, in their case after aragonite, but here we suggest such microtextures can also develop in low-Mg calcite after high-Mg calcite.

Previous work on former high-Mg calcite has provided little information on the relative timing of precipitation of low-Mg calcite and its microdolomite inclusions. Results from CC and TEM imaging in the present study suggest that microdolomite postdated calcite, and crystallized both as a cement within its micropores and by replacement. As apatite inclusions can also have a habit defined by the $\{10\bar{1}4\}$ planes of calcite (Fig. 5a, b) they are likely to have also crystallized within preexisting pore space. The late-stage timing of dolomite precipitation may be because it crystallized only after fluid Mg/Ca had reached a threshold value following removal of calcium from solution by the low-Mg calcite and apatite. The phosphorous for apatite was probably derived from organic matter originally included within the lenses, and celestite was most likely produced by combination of strontium from the high-Mg calcite with sulphur derived either from organic matter or marine-derived pore fluids.

4.3. Diagenetic modification of lens compositions

Of the three compositionally distinct lens groups, those that are rich in both magnesium and strontium belong to the Moroccan species *Austerops smoothops*, *Barrandeops granulops* and *Phacops* sp (Fig. 3), and these compositions suggest that the lenses are well preserved. It is notable that the enclosing cuticles of *A. smoothops* and *B. granulops* are similarly magnesium- and strontium-rich, but the magnesium is inferred to have been introduced during replacement by Mg-Fe phyllosilicates. It is possible that the associated lenses also gained magnesium during diagenesis. However, as the lenses of these two species contain microdolomite crystals, which are absent from calcite cuticles, they are inferred to have been richer in magnesium *in vivo*, with magnesium being introduced to the cuticles during later diagenesis. The magnesium and strontium concentrations of *Phacops* sp. lenses are very different to those in the associated cuticles and so these are interpreted to reflect original compositional contrasts.

The magnesium-poor lenses are similar in composition to their adjacent cuticles. However as microdolomite is present within lenses but absent from the cuticles, the lenses probably originally contained significantly greater concentrations of magnesium and much of it was lost during recrystallization. Loss of magnesium is the norm for diagenetic recrystallization of high-Mg calcite. For example, Carpenter et al. (1991) studied Late Devonian (Frasnian) marine cements from Australia and Canada and found average compositions of unaltered/altered cement pairs of 5.74/3.29 and

2.80/2.25 mole% $MgCO_3$. Tobin and Bergström (2002) described variably altered Upper Ordovician marine cements in which the more altered ones contained microdolomite and had 0.2 to 1.4 mole% $MgCO_3$ whereas the less altered cements were microdolomite-free with 1.3 to 3.1 mole% $MgCO_3$. Diagenetic loss of magnesium also explains why Campbell (1975) found only ~1.8 mole% $MgCO_3$ in lenses of *Eldredgeops rana milleri*, leading him to reject the possibility that they could originally have been composed of magnesium-rich calcite. It is also important to note that variability in the degree of loss of magnesium from lenses would be expected to differ significantly between rock units of different ages and from different geographical locations, and such trends were documented on a regional scale for Mississippian crinoids by Leutoff and Meyers (1984). As the *Geesops schlotheimi* lenses have relatively high strontium concentrations, which are comparable to those of their adjacent cuticles (Fig. 3), diagenesis at the Eifelian Trilobitenfelder locality is inferred to have led to loss of a greater proportion of magnesium from the lenses than strontium.

The nature of the diagenetic alteration of lens calcite can be understood better by modelling the volume of low-Mg calcite and dolomite produced by closed system recrystallization of high-Mg calcite. In the example below 1 mole of high-Mg calcite containing 7.5 mole% $MgCO_3$ (the assumed *in vivo* lens composition, see below) recrystallizes to calcian dolomite plus Mg-free calcite:

$$1Ca_{0.925}Mg_{0.075}CO_3 = 0.08Ca_{1.07}Mg_{0.93}(CO_3)_2 + 0.84CaCO_3 \quad (1)$$

The high-Mg calcite has a volume of 36.63 cm^3 and reaction products occupy a volume of 35.99 cm^3 (i.e. 5.27 cm^3 dolomite plus 30.72 cm^3 calcite) and so there is a volume reduction of 0.64 cm^3 (i.e. 1.75 %). The volume decrease predicted for closed system recrystallization of high-Mg calcite is considerably less than the 3 to 7 vol. % porosity observed in the lenses. Thus material must have been exported from the lenses during recrystallization (i.e. not a closed system). Some of this volume reduction may be accounted for by loss of organic material, which could have been an important constituent of schizochroal lenses *in vivo* (e.g. Bruton and Hass, 2003; Schoenemann and Clarkson, 2011), although a proportion of its phosphorous may have been retained in apatite. It is also likely that calcium and magnesium were exported to the host rock, and the apparent loss of magnesium from the lenses indicates that the material exported had a greater Mg/Ca ratio than the original lens.

Some lenses are uniformly turbid but most contain parts with different densities of micropores and microdolomite inclusions. This may reflect *in vivo* variations in magnesium concentrations and such an explanation was used by Lee et al. (2007) to account for the concentration of micropores and microdolomite crystals within the core and bowl of *Dalmanites sp*. lenses. For the other samples studied the only consistent intralensar differences in turbidity are in the optically clear bowls of *Austerops smoothops*, *Phacops* sp. and *Eldredgeops rana*. These bowls may represent parts of the lenses that had unusually high concentrations of magnesium *in vivo* and were dissolved rather than being replaced during diagenesis. Dissolution may have been facilitated by the position of the bowl at the base of the lens and in contact with the host rock. The magnesium-poor and iron-rich compositions of clear bowls in *Austerops smoothops* and *Phacops* sp. lenses would be consistent with the clear calcite being a burial diagenetic cement.

4.4. In vivo lens compositions

The minimum *in vivo* concentration of magnesium in lens calcite could be inferred from the threshold composition at which magnesium-bearing calcite alters during diagenesis to low-Mg calcite plus microdolomite, but there is no clear stability boundary. Dickson (2004) described fossil echinoderm stereom that had as little as ~5 mole% $MgCO_3$ *in vivo* yet had recrystallized to calcite plus microdolomite. Similarly, Carpenter et al. (1991) described marine cements that had recrystallized despite originally containing only 2.8 mole% $MgCO_3$. As the well preserved non-lensar cuticles examined in the present study have as much as ~2.4 mole% $MgCO_3$ but are free of microdolomite, the now altered lenses are assumed to have originally been significantly richer in magnesium.

The nature of diagenetic alteration of echinoderm stereom in the samples studied may be used to help infer original lens compositions. The stereom fragments in thin sections of both of the *Geesops schlotheimi* samples and the *Dalmanites* sp. sample are internally structureless and their calcite contains abundant micrometer-sized pores and microdolomite inclusions. This is typical of the 'type 2' transformation of echinoderm stereom described by Dickson (2001a) whereby *in vivo* compositions may or may not be preserved. Parts of the echinoderm fragment in the *Phacops* sp. sample also showed type 2 transformation, but most areas display 'type 1' whereby both the structure and the chemical composition of the stereom network have been preserved owing to the very fine scale of its recrystallization to calcite plus microdolomite (Dickson, 2001a). The *in vivo* chemical compositions of the stereom fragments studied must therefore be equal to or greater than the 6.15 mole% $MgCO_3$ obtained from the stereom network in the *Phacops* sp. thin section. This composition is slightly lower than the 7.5 mole% $MgCO_3$ of well preserved *Lepidocrinus multi* stereom from the Middle Devonian of the Eifel region of Germany (Dickson, 2004). If the stereom in the *Phacops* sp. thin section also contained 7.5 mole% *in vivo* then it has lost 18% of its original magnesium during recrystallization. Assuming that the *Phacops* sp. lenses have lost the same proportion of their magnesium by virtue of recrystallizing at the same time and probably in a similar diagenetic system as the stereom fragments, this would suggest that they also contained 7.5 mole% $MgCO_3$ *in vivo*. This tentative correlation between stereom and lens diagenesis is supported by the finding that together with the two other Moroccan samples the *Phacops* sp. lenses contain the smallest microdolomite crystals (Table 3). In the model of Dickson (2001a) this would suggest the finest scale of transformation of original high-Mg calcite and so these lenses should be most similar to original compositions.

Results of this study show that the lenses of schizochroal trilobite eyes crystallized as high-Mg calcite that could have contained ~7.5 mole% $MgCO_3$ whereas the non-lensar cuticle had ~2.0 to 2.4 mole% $MgCO_3$ *in vivo*. Thus the animal was able to significantly vary the partition coefficient of magnesium (D_cMg) between different parts of the cuticle that were crystallizing at approximately the same time. Formation of high-Mg calcite by these taxa is especially notable owing to the low Mg/Ca value of ambient seawater. Although the D_cMg value is likely to have varied with seawater temperature, as observed for present-day echinoderms (e.g. Dickson 2002), partition coefficients for non-lensar cuticle and lenses can be estimated by assuming Ordovician-Devonian seawater ratios of between 1.0 and 1.3 (Hardie, 1996). Calculated D_cMg values are 0.016 to 0.025 for the non-lensar cuticle and 0.062 to 0.081 for the lenses; by comparison D_cMg for present-day tropical echinoderms is only 0.032 (Dickson, 2002). These findings of such a strong biological control on the chemical

composition of lens calcite indicates that magnesium was crucial for the functioning of the optical systems of phacopine trilobites, most probably through its influence on the refractive index of calcite.

5. Conclusions

The cuticles of the analysed phacopine trilobites have undergone extensive diagenetic alteration thus complicating inferences of their original mineralogy and chemical composition. It is likely that the same would apply to any sample to some degree. The non-lensar parts of the cuticles were originally composed of low-Mg calcite and examples with higher magnesium contents are due to partial replacement by a Mg-Fe phyllosilicate. In contrast, the lenses originally contained high-Mg calcite. Magnesium concentrations may have varied within them, for example being higher in the bowl, but in most cases these intralensar structures have been erased by loss of magnesium from the lens or its redistribution on the micrometre to tens of micrometre scale during recrystallization. The best preserved lenses are from the Early Devonian of Morocco and their inferred *in vivo* compositions of ~7.5 mole% $MgCO_3$ suggest that magnesium was vital for the functioning of their optical systems.

Acknowledgements

We thank Peter Chung for help with the SEM, Billy Smith and Colin How for assistance with FIB and TEM work, Les Hill for the photographs of trilobite specimens, and Chris Hayward (University of Edinburgh) for assistance with the electron probe microanalysis. We also thank the following for providing the specimens on which this work was based: David Bruton (University of Oslo), Petr Budil (Czech Geological Survey), Brian Chatterton and Ryan McKellar (University of Alberta), Euan Clarkson (University of Edinburgh), Richard Fortey and Claire Mellish (Natural History Museum, London), Christian Klug (Museum der Universität Zürich), David Rudkin (Royal Ontario Museum) and Brigitte Schoenemann (Universität Bonn). The Leverhulme Trust is thanked for funding this research project through Research Grant F/07 179/AM. We are grateful to Brian Chatterton and Christian Klug for their careful reviews of this manuscript.

References

Blake, D.F., Peacor, D.R. Wilkinson, B.H., 1982. The sequence and mechanism of low-temperature dolomite formation: Calcian dolomites in a Pennsylvanian echinoderm. Journal of Sedimentary Research 52 (1), 59–70.

Brand, U., 2004. Carbon, oxygen and strontium isotopes in Paleozoic carbonate components: an evaluation of original seawater-chemistry proxies. Chemical Geology 204 (1-2), 23–44.

Bruton, D.L., Haas, W., 2003. The puzzling eye of *Phacops*. Special papers in Palaeontology 70, 349–361.

Campbell, K.S.W., 1975. The functional anatomy of Phacopid trilobites: Musculature and eyes. Journal and Proceedings, Royal Society of New South Wales 108, 168–188.

Carpenter, S. J., Lohmann, K.C., Holden, P., Walter, L.M., Huston, T J., Halliday, A.N., 1991. $\delta^{18}O$ values, and Sr/Mg ratios of Late Devonian abiotic marine calcite: Implications for the composition of ancient seawater. Geochimica et Cosmochimica Acta 55 (7), 1991–2010.

Clarkson, E.N.K., Levi-Setti, R.L., 1975. Trilobite eyes and the optics of Des Cartes and Huygens. Nature 254 (5502), 663–667.

Clarkson, E., Levi-Setti, R., Horvath, G., 2006. The eyes of trilobites: The oldest preserved visual system. Arthropod Structure and Development 35 (4), 247–259.

Dickson, J.A.D., 2001a. Diagenesis and crystal caskets: Echinoderm Mg calcite transformation, Dry Canyon, New Mexico, USA. Journal of Sedimentary Research 71 (5), 764–777.

Dickson, J.A.D., 2001b. Transformation of echinoid Mg calcite skeletons by heating. Geochimica et Cosmochimica Acta 65 (3), 443–454.

Dickson, J.A.D., 2002. Echinoderm skeletal preservation: Calcite/aragonite seas and the Mg/Ca ratio of Phanerozoic oceans. Science 298 (5596), 1222–1224.

Dickson, J.A.D., 2004. Echinoderm skeletal preservation: Calcite-aragonite seas and the Mg/Ca ratio of Phanerozoic oceans. Journal of Sedimentary Research 74 (3), 355–365.

Goldsmith, J.R., 1960. Exsolution of dolomite from calcite. Journal of Geology 68 (1), 103–109.

Grover, J., Kubanek, F., 1983. The formation of ordered dolomite from high-magnesium calcite at 250° to 350 °C and 1500 bars: Epitactic growth with optimal phase orientation, and implications for carbonate diagenesis. American Journal of Science 283, 514–539.

Gunderson, S.H., Wenk, H.R., 1981. Heterogeneous microstructures in oolitic carbonates. American Mineralogist 66 (7–8), 789–800.

Hardie, L.A., 1996. Secular variation in seawater chemistry: An explanation for the coupled secular variation in the mineralogies of marine limestones and potash evaporites over the past 600 my. Geology 24 (3), 279–283.

James, N.P., Klappa, C.F., 1983. Petrogenesis of early Cambrian reef limestones, Labrador, Canada. Journal of Sedimentary Petrology 53 (4), 1051–1096.

Klug, C., Schulz, H., De Baets, K., 2009. Red Devonian trilobites with green eyes from Morocco and the silicification of the trilobite cuticle. Acta Palaeontologica Polonica 54 117–123.

Lee, M.R., 2010. Transmission electron microscopy (TEM) of Earth and planetary materials: A review. Mineralogical Magazine 74, 1–27.

Lee, M.R., Bland, P.A., Graham, G., 2003. Preparation of TEM samples by focused ion beam (FIB) techniques: applications to the study of clays and phyllosilicates in meteorites. Mineralogical Magazine 67 (3), 581–592.

Lee, M.R., Torney, C., Owen, A.W., 2007. Magnesium-rich intralensar structures in schizochroal trilobite eyes. Palaeontology 50, 1031–1037.

Lee, M.R., Hodson, M.E., Langworthy, G., 2008. Earthworms produce granules of intricately zoned calcite. Geology 36 (12), 943–946.

Lohmann, K.C., Meyers, W.J., 1977. Microdolomite inclusions in cloudy prismatic calcites: a proposed criterion for former high magnesium calcites. Journal of Sedimentary Petrology 47 (3), 1078–1088.

Leutoff, A.H., Meyers, W.J., 1984. Regional distribution of dolomite inclusions in Mississippian echinoderms from southwestern New Mexico. Journal of Sedimentary Petrology 54 (2), 432–446.

Lowestam H., A., 1963. Biologic problems relating to the composition and diagenesis of sediments. In: Donnelly T.W. (Ed.) The Earth Sciences, Problems and Progress in Current Research. University of Chicago Press, pp. 137–195.

McAllister, J. E., Brand, U., 1989a. Geochemistry of some Ordovician and Devonian trilobite cuticles from North-America. Chemical Geology 78 (1), 51–63.

McAllister, J. E., Brand, U., 1989b. Primary and diagenetic microstructures in trilobites. Lethaia 22, 101–111.

Miller, J., Clarkson, E.N.K., 1980. The post-ecdysial development of the cuticle and the eye of the Devonian trilobite Phacops rana milleri Stewart 1927. Philosophical Transactions of the Royal Society of London Series B–Biological Sciences 288 (1030), 461–480.

Porter, S.M., 2010. Calcite and aragonite seas and the de novo acquisition of carbonate skeletons. Geobiology 8 (4), 256–277.

Reeder, R.J., 1992. Carbonates: growth and alteration microstructures. In: Buseck, P.R. (Ed.) Reviews in Mineralogy: Minerals and reactions at the atomic scale: Transmission electron microscopy. Mineralogical Society of America, pp. 381–424.

Rush, P.F., Chafetz, H.S., 1991. Skeletal mineralogy of Devonian stromatoporoids. Journal of Sedimentary Petrology 61 (3), 364–369.

Schoenemann, B., Clarkson, E.N.K., 2011. Light guide lenses in trilobites? Earth and Environmental Science Transactions of the Royal Society of Edinburgh 102, 17-23.

Taylor, P.D., Wilson, M.A., 1999. *Dianulites Eichwald*, 1829; an unusual Ordovician bryozoan with a high-magnesium calcite skeleton. Journal of Paleontology 73, 38–48.

Teigler, D.J., Towe, K.N., 1975. Microstructure and composition of trilobite cuticles. Fossils and Strata 4, 137–149.

Tobin, K.J., Bergström, S.M., 2002. Implications of Ordovician (~460 Myr) marine cement for constraining seawater temperature and atmospheric pCO_2. Palaeogeography Palaeoclimatology Palaeoecology 181 (4), 399–417.

Torney, C., Lee, M.R., Owen, A.W., 2008. An electron backscatter diffraction study of Geesops: A broader view of trilobite vision? In: Rábano, I., Gozalo R., Garcia-Bellido, G. (Eds.) Advances in Trilobite Research. Cuadernos del Museo Geominero 9, 389–393.

Towe, K.M., 1973. Trilobite eyes: Calcified lenses in vivo. Science 179 (4077), 1007–1009.
Webb, G.E., Sorauf, J.E., 2002. Zigzag microstructure in rugose corals: A possible indicator of relative seawater Mg/Ca ratios. Geology 30 (5), 415–418.
Wilmot, N.V., Fallick, A.E., 1989. Original Mineralogy of trilobite cuticles. Palaeontology 32 (2), 297–304.
Wilmot, N.V., 1990. Primary and diagenetic microstructures in trilobite cuticles. Historical biology 4 (1), 51–65.
Zhuravlev, A.Y., Wood, R.A., 2008. Eve of biomineralization: Controls on skeletal mineralogy. Geology 36 (12), 923–926.

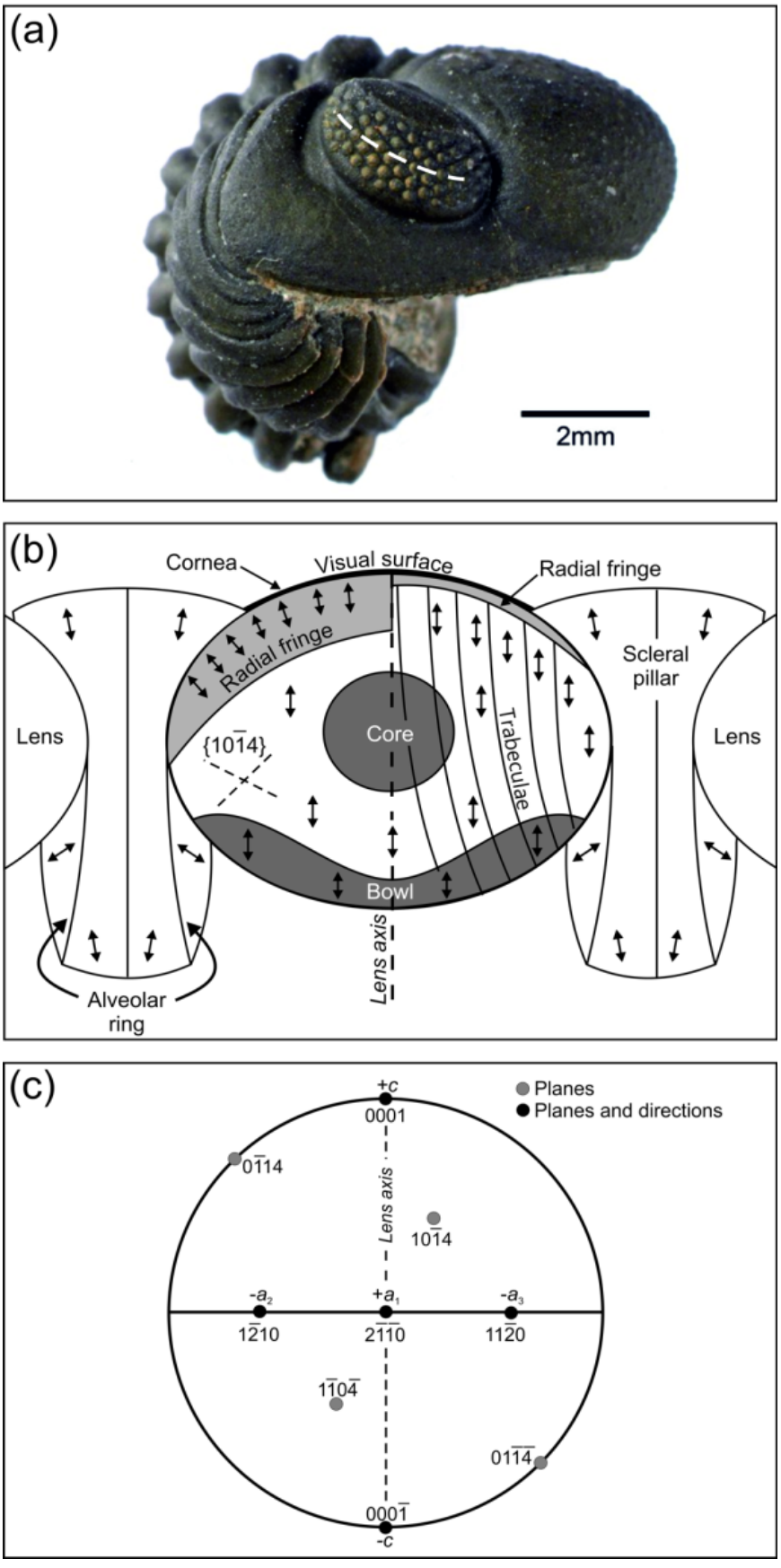
(a)
2mm
(b)
Cornea
Visual surface
Radial fringe
Radial fringe
Scleral pillar
Lens
Lens
Core
{10$\bar{1}$4}
Trabeculae
Bowl
Lens axis
Alveolar ring
(c)
Planes
Planes and directions
+c
0001
0$\bar{1}$14
Lens axis
10$\bar{1}$4
-a_2
+a_1
-a_3
1$\bar{2}$10
2$\bar{1}\bar{1}$0
11$\bar{2}$0
1$\bar{1}$04
01$\bar{1}\bar{4}$
000$\bar{1}$
-c

Fig. 1. (a) Lateral view of enrolled specimen of *Austerops smoothops* showing the right eye. Thin sections were prepared in an orientation approximately normal to the plane of the page and parallel to palpebral lobe as indicated by the dashed white line. (b) Schematic diagram showing the features of the two main lens types found in this study. The orientation of the calcite *c* axis is indicated by the double headed arrows. The right hand side of the lens shows microstructures characteristic of the samples of *Dalmanites* sp. and *Odontochile hausmanni* whereby calcite *c* axes lie parallel to the lens axis throughout all of the lens apart from a very thin radial fringe immediately beneath the visual surface. Within the radial fringe calcite *c* axes fan outwards towards the visual surface. These lenses can also contain elongate subgrains whose curving boundaries make trabeculae that are visible in transmitted light. The left hand side shows microstructures of lenses in most of the other species studied whereby there is a much thicker radial fringe and although calcite in the lens center is oriented with its *c* axis parallel to the lens axis, *c* axes may also fan out towards the lens base (not shown). The core and bowl are most readily recognised in transmitted light and by their contrasts in turbidity with the rest of the lens. They may be seen in either type of lens, but rarely together in the same one. Most lenses are between 100 and 200 μm in maximum horizontal diameter. (c) Upper hemisphere stereographic projection showing the crystallographic orientation of calcite along the lens axes of both lens types. This projection assumes that the plane of the thin section was precisely along the lens axis and in the 'horizontal' plane, parallel to the palpebral lobe. In practice most thin sections were cut at a shallow angle to the lens axis and inclined to the horizontal plane so that for any one lens the positions of the planes and directions may differ from the idealised example shown.

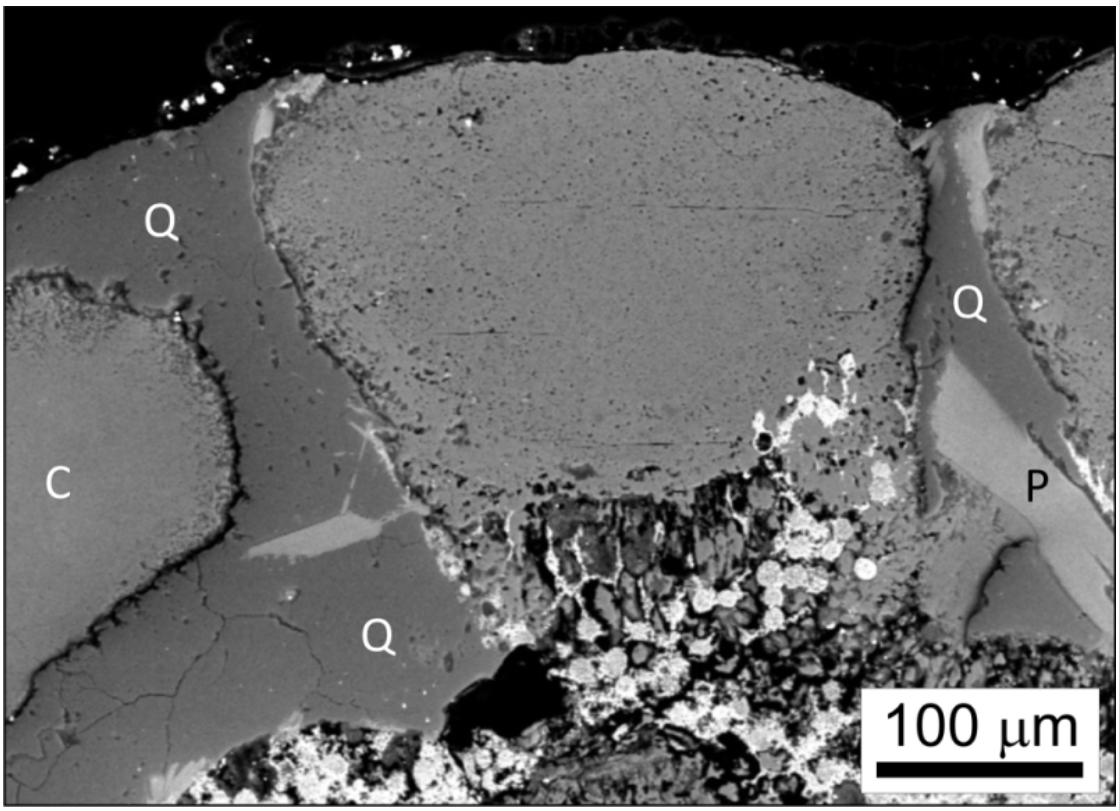

Fig. 2. BSE image of part of the eye of *Barrandeops granulops*. A lens is in the center of the image and the host rock beneath contains abundant framboidal pyrite (white). The sclera separating this lens from the one on the right hand edge of the image has been replaced by quartz (Q, medium grey) and a lath-shaped Mg-Fe phyllosilicate (P), as has part of the cuticle (C) to the left of the central lens.

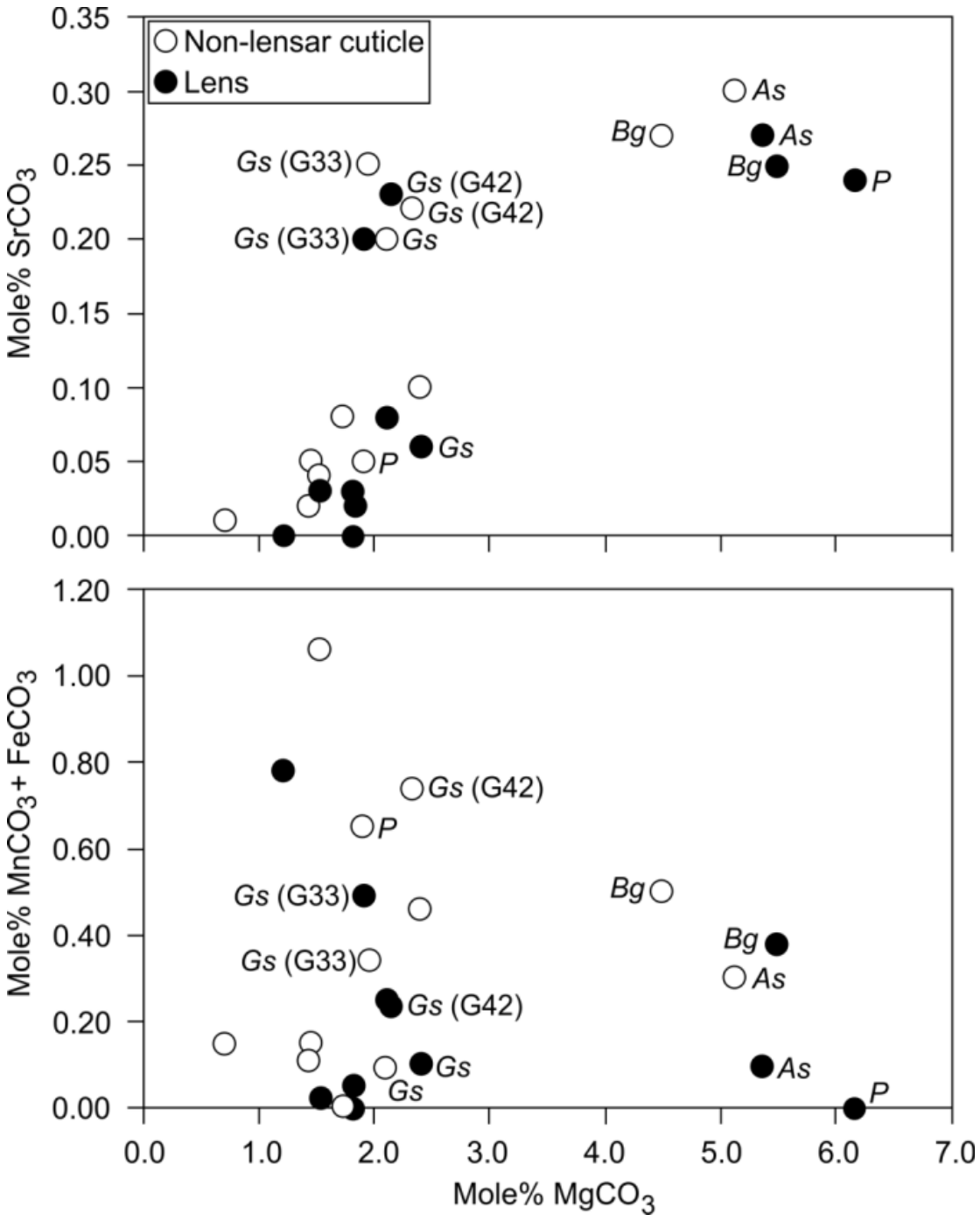

Fig. 3. Plots of the chemical compositions of lenses and non-lensar cuticle of the eleven species studied. These data are also listed in Table 2. The datapoints corresponding to the three Morroccan species *Austerops smoothops, Barrandeops granulops and Phacops* sp. are indicated by *As*, *Bg* and *P* respectively, the datapoints for the two samples of *Geesops schlotheimi* are labelled *Gs* (G42) and *Gs* (G33), and the datapoints for the sample of *Geesops sparsinodosus* are labelled *Gs.*

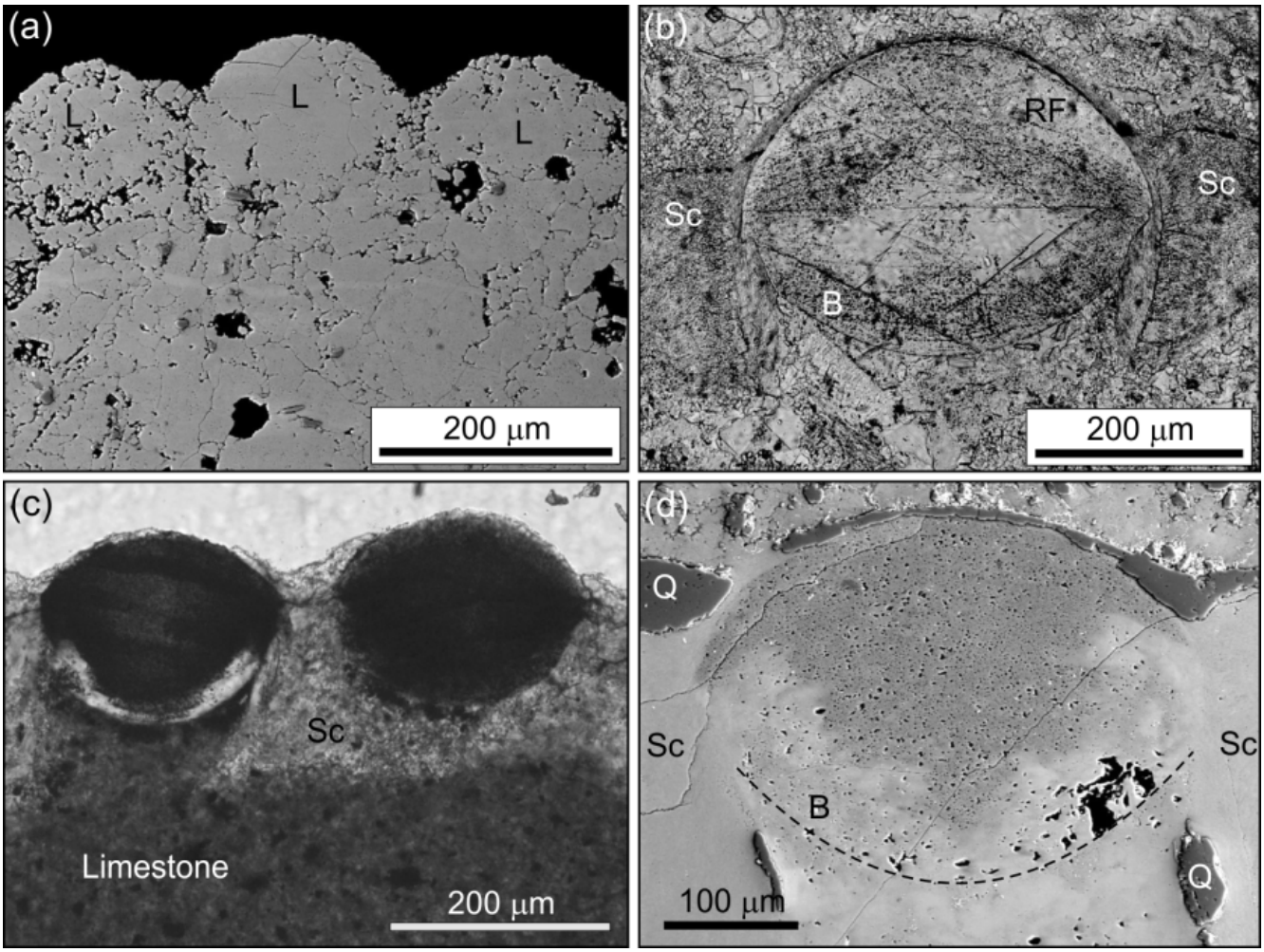

Fig. 4. (a) BSE image of *Reedops cephalotes* showing three lenses (L) that are distinguished by their convex visual surfaces and are composed of equant calcite crystals. The intervening sclera has been recrystallized to the extent that is microstructure is no longer recognisable. (b) Plane polarised transmitted light image of a *Reedops* cf. *cephalotes* lens and sclera (Sc). The bowl (B) and radial fringe (RF) are turbid whereas the core is optically clear. The fine lines within the lens are $\{10\bar{1}4\}$ cleavages and $\{\bar{1}018\}$ *e* twins, both of which are present in multiple orientations. EBSD shows that the thin section has been cut such that the *c* axis of lens calcite lies at 19º the plane of the page and $<10\bar{1}0>$ is normal to the page. (c) Plane polarised transmitted light image of *Austerops smoothops* showing two lenses separated by sclera (Sc) with limestone beneath. The lenses are turbid apart for a thin clear bowl in the left hand lens. (d) BSE image of a *Phacops* sp. lens. The central and upper part of the lens contains abundant micropores and microdolomite crystals whereas the large bowl (B) is free of microdolomite but contains some irregular pores (black). The base of the lens is indicated by a dashed line. The cornea and parts of the sclera (Sc) have been replaced by quartz (Q).

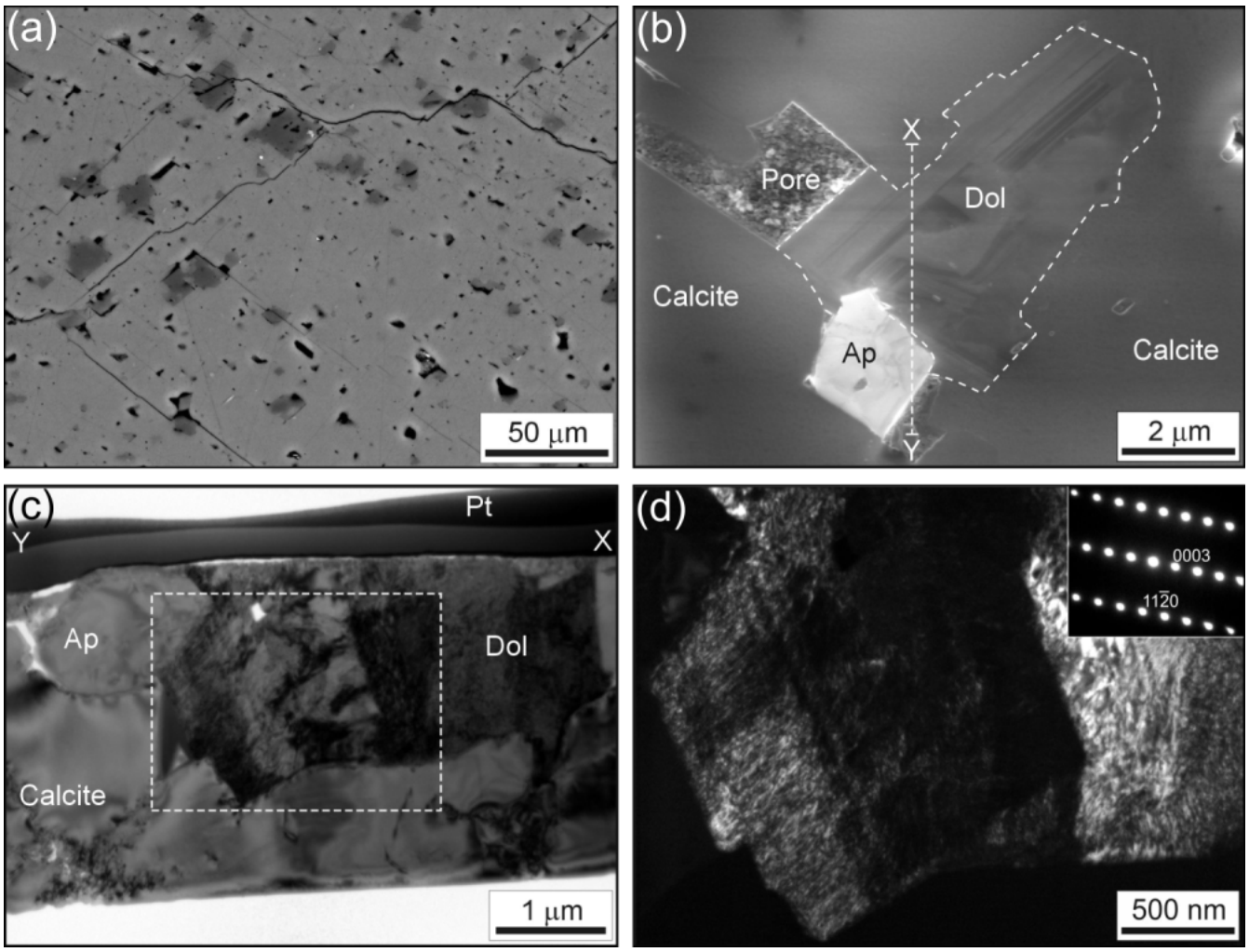

Fig. 5. (a) BSE image of the interior of a *Boeckops boecki* lens that is composed of calcite (light grey) with micropores (black) and inclusions of microdolomite (dark grey). The fine straight lines are the $\{10\bar{1}4\}$ calcite cleavage planes. (b) CC image of *Dalmanites* sp. lens calcite containing a micropore together with microdolomite (Dol) and apatite (Ap) inclusions. The *c* axis of calcite is oriented N-S in the image. The edges of the microdolomite crystal are delineated by a dashed white line. The boundaries of the micropore and faces of the microdolomite and apatite crystals are parallel or near-parallel to the calcite $\{10\bar{1}4\}$ cleavage planes (oriented NE-SW and NW-SE). Zones in the microdolomite crystal (aligned NE-SW) are also parallel to $\{10\bar{1}4\}$. Note that the microdolomite crystal has grown into the lower part of the pore. (c) Bright-field TEM image of a foil cut from along the line X-Y in (b). The microdolomite crystal (Dol) is oriented such that the electron beam is close to its $[\bar{1}100]$ zone axis and so is scattering electrons strongly (i.e. dark). The microdolomite partly encloses and so postdates the apatite (Ap) crystal. (d) Dark-field TEM image of the boxed area in (c). The image was formed using the dolomite 0003 reflection and highlights its fine-scale modulated microstructure. The dark bands oriented NNW-SSE lie parallel to a crystal face and contain dolomite whose modulations are of a different scale or orientation, and these bands probably correspond to the compositional zones seen in the CC image. The $[\bar{1}100]$ SAED pattern is inset.

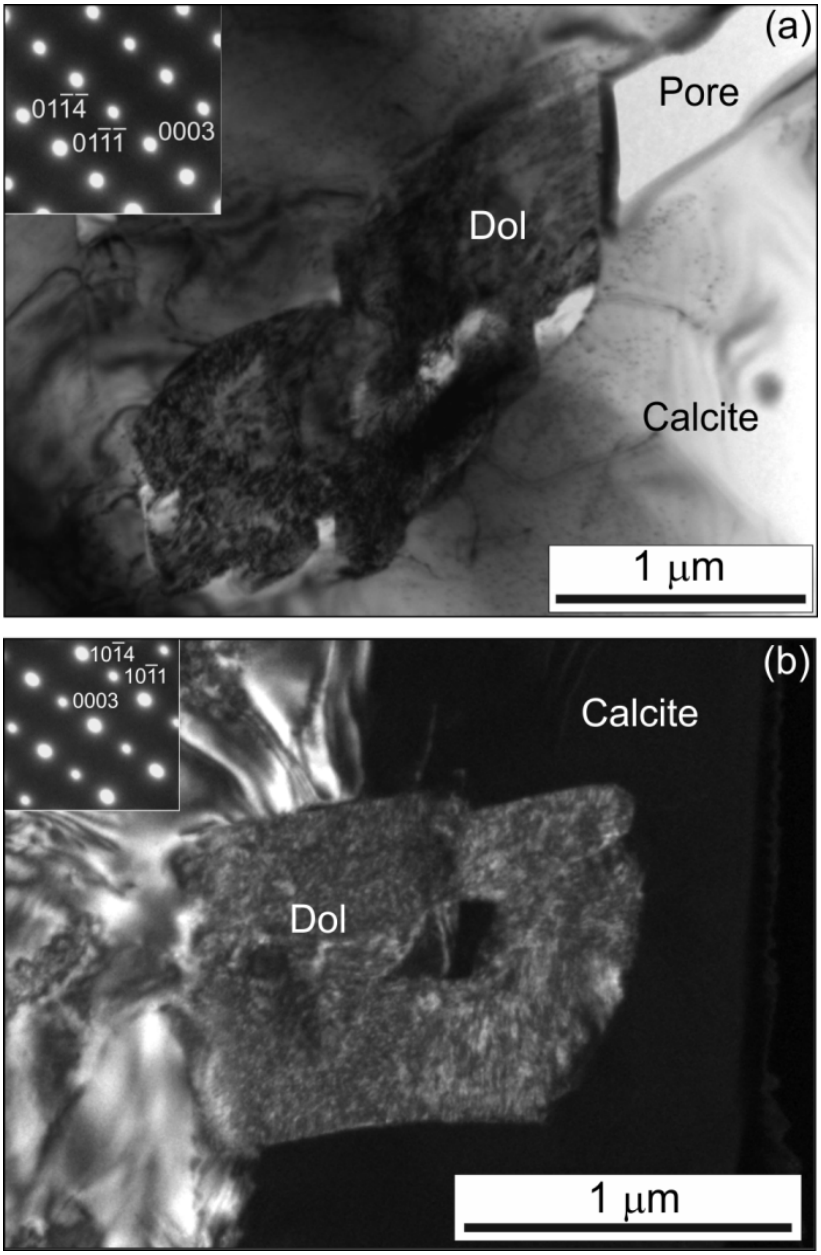

Fig. 6. (a) Bright-field TEM image of a microdolomite crystal (Dol) from the *Reedops* cf. *cephalotes* lens in Figure 4b that has crystallized within an elongate micropore enclosed by calcite. The inset $[2\bar{1}\bar{1}0]$ SAED pattern of the microdolomite shows that those crystal faces that are oriented approximately N-S lie parallel to the trace of $(01\bar{1}\bar{4})$. (b) Dark-field TEM image of a microdolomite crystal (Dol) within *Geesops sparsinodosus* lens calcite made using the superimposed 0006 reflections of calcite and dolomite. The microdolomite has a very fine-scale modulated microstructure. It cross-cuts the boundary between two calcite subgrains that differ slightly in orientation, and also has an inclusion of calcite in its center. The faces of the microdolomite crystal that lie roughly E-W in the image are parallel to the trace of the $(10\bar{1}4)$ plane. The inset $[1\bar{2}10]$ SAED pattern is made from both dolomite and its enclosing calcite and shows that both minerals are in precisely the same crystallographic orientation so that reflections from the two patterns are superimposed.

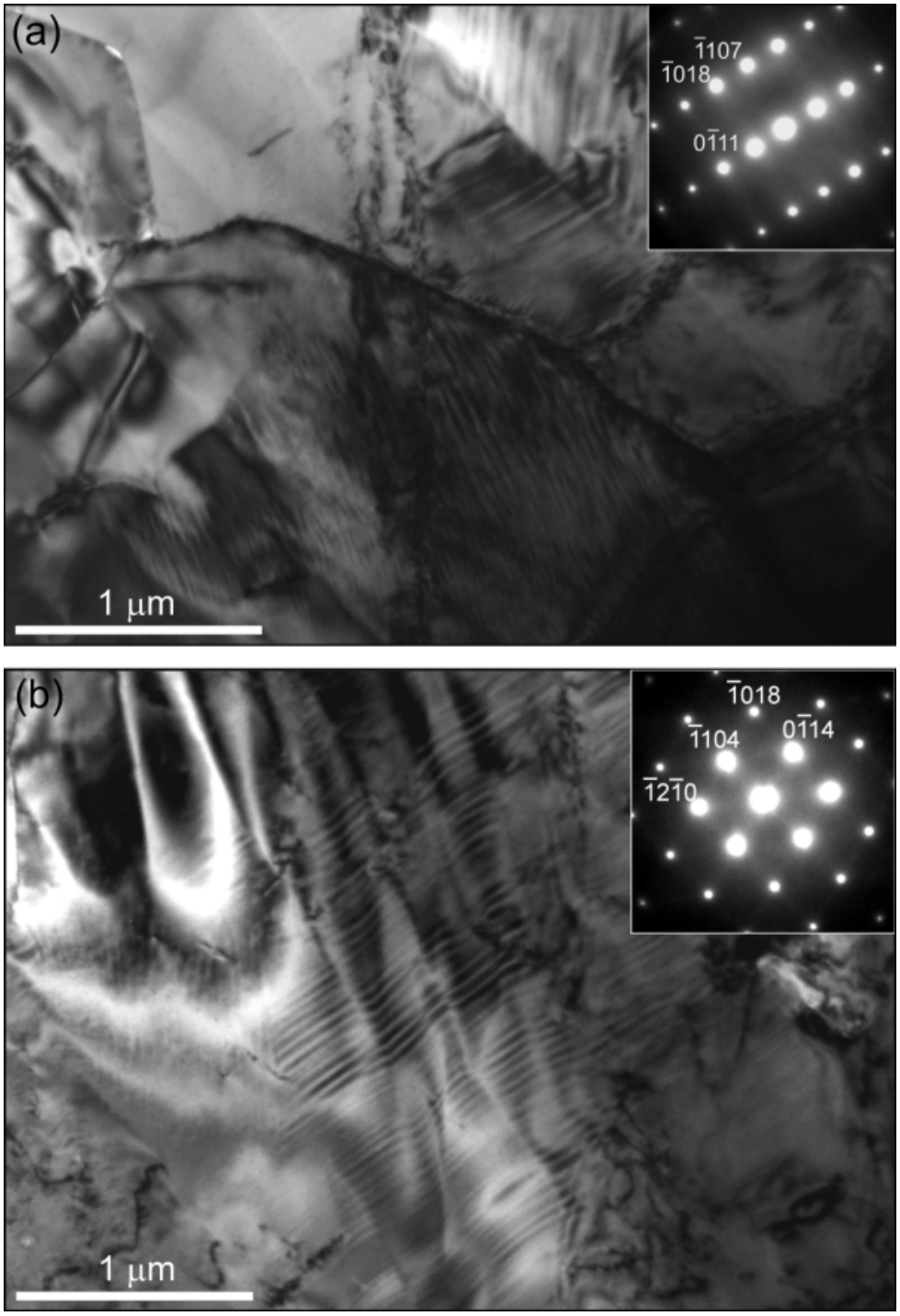

Fig. 7. Bright-field TEM images of the interior of the *Reedops* cf. *cephalotes* lens in Figure 4b. (a) An area of calcite with several subgrains that have dislocation-rich boundaries and contain ~30 nm scale modulations. Note that the modulations in the upper right are rotated by a twin plane, probably a $\{\bar{1}018\}$ *e* twin. The corresponding $[5\bar{2}\bar{3}1]$ SAED pattern is inset. (b) Bright-field image of calcite containing ~30 nm sized modulations that are oriented parallel to the trace of $(\bar{1}104)$. The corresponding $[40\bar{4}1]$ SAED pattern (inset) shows streaking between spots produced by the lamellar microstructures.

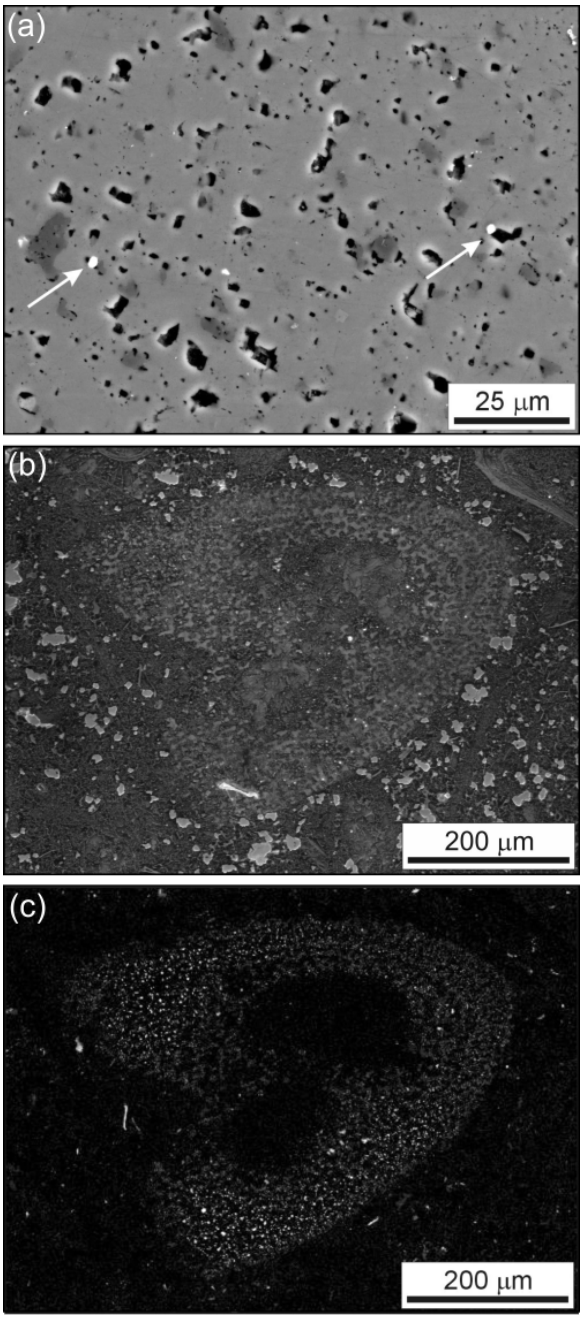

Fig. 8. (a) BSE image of the interior of a fragment of echinoderm stereom from the *Geesops schlotheimi* (G33RT) thin section. It is composed of calcite (light grey) with abundant micropores (black), together with inclusions of microdolomite (dark grey) and celestite (white, arrowed). (b) CC image of a stereom fragment from the *Phacops* sp. thin section illustrating the good preservation of the stereom network. The angular light grey grains surrounding the stereom fragment are detrital quartz. (c) Mg K_{α} X-ray map of the field of view in (b) highlighting the distribution of microdolomite. Within most of the stereom fragment the microdolomite crystals are too small to individually resolve but are coarser in the lower left and upper left parts of the stereom.

Table 1
List of the trilobite species studied, their sampling locality, stratigraphic position and nature of their host rock.

Species	Sampling locality	Stratigraphic position	Host rock
Dalmanites sp. TS1, TS3	Unknown	Unknown	Wackestone including fragments of echinoderm stereom
Eldredgeops rana	Martin-Marietta Quarry, Milan, Michigan, USA (45° 05′ N 83° 41′ W)	Middle Devonian (Giventian) Silica Fm	Partially dolomitized wackestone
Geesops schlotheimi G31R, G33RT, G41R, G42	Eifelian Trilobitenfelder, Gees, Eifel, Germany (50° 13′ 13″ N 6° 41′ 20″ E)	Middle Devonian (lower Eifelian) Ahrdorf Fm	Wackestone including fragments of echinoderm stereom
Geesops sparsinodosus	Eifelian Trilobitenfelder, Gees, Eifel, Germany (50° 13′ 13″ N 6° 41′ 20″ E)	Middle Devonian (lower Eifelian) Ahrdorf Fm	Wackestone
Phacops sp.	Jbel Gara el Zguilma, Morocco (29°45′04.7″N 06°42′20.2″W)	Early-Middle Devonian (Late Emsian-Upper Eifelian) Terarine Fm	Carbonate mudstone including fragments of echinoderm stereom
Barrandeops granulops	Hamar Laghdad, Tafilalt, Morocco (31° 22′ 37′ N 4° 03′ 28″ W)	Early-Middle Devonian (Late Emsian-Upper Eifelian) Timrhanrhart Fm	Carbonate mudstone
Austerops smoothops	Jbel Gara el Zguilma, Morocco (29°45′04.7″N 06°42′20.2″W)	Early-Middle Devonian (Late Emsian-Upper Eifelian) Timrhanrhart Fm	Carbonate mudstone
Reedops cephalotes	Konvarka (Praha-Smichov), Czech Republic (50° 03′ 09″ N 14° 24′ 10″ E)	Early Devonian (Pragian) Praha Fm, Dvorce-Prokop Limestone Facies	Wackestone
Reedops cf *cephalotes*	Konvarka (Praha-Smichov), Czech Republic (50° 03′ 09″ N 14° 24′ 10″ E)	Early Devonian (Pragian) Praha Fm, Dvorce-Prokop Limestone Facies	Wackestone
Odontochile hausmanni	Konvarka (Praha-Smichov), Czech Republic (50° 03′ 09″ N 14° 24′ 10″ E)	Early Devonian (Pragian) Praha Fm, Dvorce-Prokop Limestone Facies	Wackestone
Boeckops boecki	Branzovy near Lodenice, Czech Republic (49° 59′ 02″ N 14° 10′ 45″ E)	Early Devonian (Pragian) Praha Fm, Loděnice Limestone Facies	Grainstone with lenses overgrown by radiaxial-fibrous cements

Where more than one sample of the same species from the same locality was studied, the different samples are indicated by their thin section number.

Table 2
Mean chemical compositions of non-lensar cuticle and lenses

Species	$CaCO_3$	$MgCO_3$	$MnCO_3$	$FeCO_3$	$SrCO_3$	n	Method
			Non-lensar cuticle (mole%)				
Dalmanites sp. (TS1)	97.04 (1.14)	2.40 (1.11)	0.09 (0.06)	0.37 (0.15)	0.10 (0.01)	21	EP
Eldredgeops rana	98.35 (0.22)	1.46 (0.24)	0.08 (0.03)	0.06 (0.04)	0.05 (0.01)	30	EP
Geesops schlotheimi (G33RT)	97.46 (0.50)	1.95 (0.50)	0.07 (0.03)	0.27 (0.05)	0.25 (0.05)	12	EP
Geesops schlotheimi (G42)	96.72 (2.68)	2.33 (1.34)	0.01 (0.03)	0.73 (1.42)	0.22 (0.09)	25	EP
Geesops sparsinodosus	97.61 (0.19)	2.10 (0.20)	0.00 (0.00)	0.09 (0.10)	0.20 (0.07)	6	AEM
Phacops sp.	97.38 (0.51)	1.91 (0.47)	0.13 (0.11)	0.52 (0.44)	0.05 (0.08)	11	AEM
Barrandeops granulops	94.73 (0.59)	4.50 (0.57)	0.13 (0.10)	0.37 (0.14)	0.27 (0.03)	5	AEM
Austerops smoothops	94.27 (0.51)	5.14 (0.54)	0.03 (0.05)	0.27 (0.11)	0.30 (0.04)	5	AEM
Reedops cephalotes	97.37 (0.29)	1.53 (0.30)	0.30 (0.09)	0.76 (0.10)	0.04 (0.05)	5	AEM
Reedops cf. *cephalotes*	98.44 (0.26)	1.43 (0.25)	0.02 (0.05)	0.09 (0.13)	0.02 (0.05)	5	AEM
Odontochile hausmanni	98.19 (0.20)	1.73 (0.21)	0.00 (0.00)	0.00 (0.00)	0.08 (0.09)	7	AEM
Boeckops boecki	99.14 (0.20)	0.70 (0.25)	0.06 (0.06)	0.09 (0.09)	0.01 (0.02)	29	EP
			Lenses (mole%)				
Dalmanites sp. (TS1)	97.56 (2.06)	2.11 (1.96)	0.03 (0.04)	0.22 (0.22)	0.08 (0.06)	68	EP
Eldredgeops rana	98.09 (0.42)	1.83 (0.41)	0.02 (0.03)	0.03 (0.07)	0.02 (0.03)	53	EP
Geesops schlotheimi (G33RT)	97.41 (1.24)	1.91 (1.15)	0.10 (0.07)	0.39 (0.16)	0.20 (0.07)	21	EP
Geesops schlotheimi (G42)	97.35 (1.04)	2.15 (0.96)	0.01 (0.04)	0.26 (0.17)	0.23 (0.05)	99	EP
Geesops sparsinodosus	97.43 (0.37)	2.41 (0.36)	0.00 (0.00)	0.10 (0.15)	0.06 (0.09)	5	AEM
Phacops sp.	93.58 (0.34)	6.18 (0.34)	0.00 (0.00)	0.00 (0.00)	0.24 (0.13)	6	AEM
Barrandeops granulops	93.87 (2.50)	5.50 (2.52)	0.08 (0.18)	0.30 (0.57)	0.25 (0.07)	52	EP
Austerops smoothops	94.24 (0.91)	5.38 (0.95)	0.04 (0.07)	0.06 (0.11)	0.27 (0.10)	7	AEM
Reedops cephalotes	97.99 (0.27)	1.21 (0.20)	0.18 (0.11)	0.60 (0.12)	0.03 (0.06)	5	AEM
Reedops cf. *cephalotes*	98.19 (0.28)	1.81 (0.28)	0.00 (0.00)	0.00 (0.00)	0.00 (0.00)	7	AEM
Odontochile hausmanni	98.11 (0.22)	1.81 (0.15)	0.00 (0.00)	0.05 (0.11)	0.03 (0.06)	10	AEM
Boeckops boecki	98.42 (2.58)	1.52 (2.58)	0.00 (0.02)	0.02 (0.08)	0.03 (0.02)	45	EP

Figures in parentheses are standard deviations.
n denotes number of analyses
Methods used for chemical analysis were electron probe microanalysis (EP) and analytical scanning electron microscopy (AEM)

Table 3
Sizes of lens microdolomite crystals.

Species	Crystal size (μm)		Number of crystals measured
	Range	Mean	
Dalmanites sp.			
TS1 lens 1	0.8 – 29.3	6.3	30
TS1 lens 2	0.5 – 13.7	2.7	20
Geesops schlotheimi			
G31R lens 1	0.7 – 6.5	2.3	33
G41 lens 1	0.5 – 11.9	3.0	43
Phacops sp.			
Lens 1	0.5 – 2.6	1.2	21
Barrandeops granulops			
Lens 1	0.3 – 5.1	1.2	64
Lens 2	0.4 – 7.1	2.1	32
Lens 3	0.4 – 8.1	2.7	35
Austerops smoothops			
Lens 1	0.4 – 5.5	1.4	30
Reedops cf. *cephalotes*			
Lens 1	0.4 – 3.4	1.4	40
Lens 2	0.4 – 3.0	1.4	13
Odontochile hausmanni			
Lens 1	0.5 – 9.7	3.4	17
Lens 2	0.7 – 5.0	2.4	12
Boeckops boecki			
Lens 1	0.5 – 34.6	5.5	26
Lens 2	0.6 – 12.9	4.0	39